Magnetocaloric effect and magnetic cooling near a field-induced quantum-critical point

Bernd Wolf[a,1], Yeekin Tsui[a,2], Deepshikha Jaiswal-Nagar[a], Ulrich Tutsch[a], Andreas Honecker[b], Katarina Remović-Langer[a], Georg Hofmann[a], Andrei Prokofiev[c], Wolf Assmus[a], Guido Donath[d], and Michael Lang[a]

[a]Physics Institute, Goethe-University, Max-von-Laue Strasse 1, 60438 Frankfurt(M), Germany;

[b]Institute for Theoretical Physics, Georg-August-University Göttingen, Friedrich-Hund-Platz 1, 37077 Göttingen, Germany;

[c]Institute of Solid State Physics, Vienna University of Technology, Wiedner Hauptstrasse 8-10, 1040 Vienna, Austria;

[d]Max-Planck-Institut for Chemical Physics of Solids, Nöthnitzer Strasse 40, 01187 Dresden, Germany;

[1]To whom correspondence may be addressed. E-mail: wolf@physik.uni-frankfurt.de

[2]Present address: Department of Physics, Durham University, United Kingdom

Classification: Physical Sciences/Physics

PNAS (2011)
doi:10.1073/pnas.1017047108

Abstract

The presence of a quantum critical point (QCP) can significantly affect the thermodynamic properties of a material at finite temperatures *T*. This is reflected, e.g., in the entropy landscape *S*(*T*, *r*) in the vicinity of a QCP, yielding particularly strong variations for varying the tuning parameter *r* such as pressure or magnetic field *B*. Here we report on the determination of the critical enhancement of $\partial S/\partial B$ near a *B*-induced QCP via absolute measurements of the magnetocaloric effect (MCE), $(\partial T/\partial B)_S$, and demonstrate that the accumulation of entropy around the QCP can be used for efficient low-temperature magnetic cooling. Our proof of principle is based on measurements and theoretical calculations of the MCE and the cooling performance for a Cu^{2+}-containing coordination polymer, which is a very good realization of a spin-½ antiferromagnetic Heisenberg chain – one of the simplest quantum-critical systems.

\body

Introduction

The magnetocaloric effect (MCE), i.e. a temperature change in response to an adiabatic change of the magnetic field, has been widely used for refrigeration. Although, up until now applications have focussed on cryogenic temperatures (1-3), possible extensions to room temperature have been discussed (4). The MCE is an intrinsic property of all magnetic materials in which the entropy S changes with magnetic field B. Paramagnetic salts have been the materials of choice for low-temperature refrigeration (1), including space applications (5-7), with an area of operation ranging from about one or two degrees Kelvin down to some hundredths or even thousandths degree Kelvin. Owing to their large $\Delta S/\Delta B$ values, the ease of operation, and the applicability under microgravity conditions, paramagnets have matured to a valuable alternative to ^{3}He-^{4}He dilution refrigerators, the standard cooling technology for reaching sub-Kelvin temperatures.

A large MCE also characterizes a distinctly different class of materials, where the low-temperature properties are governed by pronounced quantum many-body effects. These materials exhibit a B-induced quantum-critical point (QCP) – a zero-temperature phase transition –, and the MCE has been used to study their quantum criticality (8, 9, 10, 11, 12, 13, 14) or to determine their B-T phase diagrams (15, 16, 17, 18, 19). The aim of the present work is to provide an accurate determination of the enhanced MCE upon approaching a B-induced QCP both as a function of B and T and to explore the potential of this effect for magnetic cooling.

Materials in the vicinity of a QCP have been of particular current interest, as their properties reflect critical behavior arising from quantum fluctuations instead of thermal fluctuations which govern classical critical points (20). Prominent examples of findings made here include the intriguing low-temperature behaviors encountered in some heavy-fermion metals, itinerant transition metal magnets (21 and references cited therein, 22) or magnetic insulators (23, 24) and the occurrence of new quantum phases near a QCP (25, 26, 10). Generally, a QCP is reached upon tuning an external parameter r such as pressure or magnetic field to a critical value. Although the critical point is inaccessible by experiment, its presence can affect the material's properties at finite temperature significantly. The thermodynamic properties are expected to show anomalous power-laws as a function of temperature and, even more spectacular, to exhibit an extraordinarily high sensitiveness on these tuning parameters (27, 28). Upon approaching a pressure (p)-induced QCP, for example, the thermal expansion coefficient $\alpha \propto \partial S/\partial p$ is more singular than the specific heat $C = T\cdot\partial S/\partial T$, giving rise to a diverging Grüneisen ratio $\Gamma_p \propto \alpha/C$ (27, 29). Likewise, for a B-induced QCP, a diverging $\Gamma_B = -C^{-1}\cdot(\partial S/\partial B)_T$ is expected (27, 28, 30) and has recently been reported (14). Unlike Γ_p, however, where experimental access, apart from measurements of the critical contributions of the two quantities α and C, is very difficult, Γ_B can be determined directly via the magnetocaloric effect (MCE) by probing temperature changes of the material in response to changes of the magnetic field B under adiabatic conditions,

$$\Gamma_B = \frac{1}{T}\left(\frac{\partial T}{\partial B}\right)_S . \qquad (1)$$

In this work, we directly measure the critical enhancement of Γ_B near a B-induced QCP and demonstrate that this effect can be used for magnetic refrigeration over an extended range

of temperatures. Our results indicate that quantum critical materials open up new possibilities for realizing very efficient and flexible low-temperature coolants.

The model substance

For the proof of principle, it is helpful to focus on simple model substances, characterized by a small number of material parameters which are well under control. One of the simplest quantum-critical systems, where an enhanced MCE (30, 28) and a potential use for magnetic cooling (31) have been predicted, is the uniform spin-½ antiferromagnetic Heisenberg chain (AFHC), described by

$$H = J\sum_i \vec{S}_i \cdot \vec{S}_{i+1}. \qquad (2)$$

This model, and its highly non-trivial physics, contains a single parameter J – the Heisenberg exchange interaction – by which nearest-neighbor spins interact along one crystallographic direction. In fact, by exploring the quasi-1D spin-½ Heisenberg antiferromagnet $KCuF_3$, it has been demonstrated that quantum-critical Luttinger liquid (LL) behavior governs the material's properties over wide ranges in temperature and energy (24). The AFHC remains in the LL quantum-critical state also in magnetic fields (32) up to the saturation field B_s, given by $g\mu_B B_s = 2J$, with g the spectroscopic g factor and μ_B the Bohr magneton. Since the fully polarized state above B_s is a new eigenstate of the system, different from that of the LL, B_s marks the endpoint of a quantum-critical line in the B-T plane.

For exploring the MCE around B_s, we use a copper-containing coordination polymer $[Cu(\mu\text{-}C_2O_4)(4\text{-aminopyridine})_2(H_2O)]_n$ (abbreviated to CuP henceforth), a good realization of a spin-½ AFHC, and compare the results with model calculations for the idealized system. In

CuP, first synthesized by Castillo *et al.* (33), Cu^{2+} (spin-½) ions, bridged by oxalate molecules (C_2O_4), form chains along the crystallographic *c*-axis (33, 34). High-quality single crystals of CuP with a small concentration n = 0.4 – 1 % of uncoupled spin-½ impurities, made recently available by a slow-diffusion technique (34), were used for the present investigations (see *SI Text I*). The magnetic susceptibility of these single crystals for $T \geq 0.055$ K, are well described by the model of a spin-½ AFHC (35) with an *intra*-chain coupling $J/k_B = (3.2 \pm 0.1)$ K (34).

In order to fully characterize the magneto-thermal properties of CuP, measurements of the specific heat $C_B(T)$ and low-temperature magnetic susceptibility $\chi_T(B)$ have been carried out (Fig. 1). The excellent agreement of these results with model calculations (solid lines in Fig. 1) (see *SI Text II*) confirms the assertion (33, 34) that CuP is a very good realization of a uniform spin-½ AFHC. Compared to other model substances of this kind, such as copper pyrazin dinitrate (36), however, CuP excels by its moderate size of *J* and the correspondingly small saturation field of 4.09 T (for $B \parallel b$), enabling the MCE to be studied in the relevant field range below about twice ([§]) the saturation field by using standard laboratory magnets.

Absolute measurements of the magnetocaloric effect and comparison with theory

For a quantitative determination of Γ_B, a novel step-like measuring technique was employed (see *SI Text III and IV*) ensuring, to good approximation, adiabatic conditions. The Γ_B data obtained this way for two different temperatures exhibit negative values for $B < B_s$ (Fig. 2A), implying that here cooling is achieved through magnetization! Upon increasing the

[§] At high magnetic fields, i.e. $B > 2 \cdot B_s$, the spin-½ AFHC behaves essentially like a paramagnet, where *T* varies linearly with *B* at *S* = const. For fields lower than about twice B_s deviations from linearity become visible (30), indicating the influence of quantum critical fluctuations.

field, Γ_B passes through a weak minimum, changes sign and adopts a pronounced maximum at fields somewhat above 4 T. The large positive Γ_B values here indicate that in this B-T range, a pronounced cooling effect is obtained through demagnetization. The sign change in $\Gamma_B \propto \partial S/\partial B$ within a narrow B-interval centered near B_s implies the presence of a distinct maximum in $S_T(B)$ – a clear signature of a nearby B-induced QCP (28). It reflects the accumulation of entropy due to the competing ground states separated by the QCP. The data taken at 0.32 K show extrema in Γ_B which are distinctly sharper and more pronounced as compared to the signatures in the 0.97 K data, suggesting incipient divergencies of Γ_B on both sides of B_s. Theoretical calculations of Γ_B have been performed for the ideal spin-½ AFHC with J/k_B = 3.2 K (solid lines in Fig. 2A). The model curves capture the essential features of the experimental results and even provide a good quantitative description for the data taken at 0.97 K. However, some systematic deviations become evident which increase with decreasing temperature: the extrema in $|\Gamma_B|$ as a function of field at fixed temperature (Fig. 2A) are less strongly pronounced compared to theoretical results and the experimental data at T = 0.32 K exceed the theory curves at high fields ($B \geq 5$ T). To follow the evolution of the extrema as a function of temperature, measurements at B = const. have been performed (insert of Fig. 2B). The deviations from the model curves suggest that by the application of a magnetic field, the divergence in $\Gamma_B(T \rightarrow 0)$ becomes truncated by the occurrence of a small energy scale, accompanied by a shift of entropy to higher fields. A plausible explanation for these observations would be the opening of a small field-induced gap. It may result, e.g., from a finite Dzyaloshinskii-Moriya (DM) interaction (38, 39) permitted by the lack of a center of inversion symmetry in CuP (33). In fact, indications for a finite DM interaction can be inferred

from measurements performed under different field orientations ([**]). According to ref. 38 the value of the DM-vector **D** can be estimated by $|\mathbf{D}| \sim (\Delta g/g)\cdot J$, where g is the material's g-factor and Δg its deviation from the free electron value. For CuP the corresponding energy scale is estimated to $|D| \sim 0.07\ J \sim 0.22\ \mathrm{K}\cdot k_B$, which exceeds the one resulting from dipole-dipole interactions by more than one order of magnitude ([††]). In addition, part of the deviations from the model curves at low temperatures can also be due to the presence of weak inter-chain interactions and the accompanied dimensional crossover, inevitable in any three-dimensional material. It may also in part reflect the influence of an enhanced thermal boundary resistance between sample and thermometer due to an enhanced spin-phonon interaction caused by a nearby phase transition (40).

Magnetic cooling and performance characteristics

Despite these deviations from the idealized system, the enhanced MCE (Fig. 2A) highlights distinct quantum-critical behavior in CuP over extended ranges of temperature and magnetic field. The strongly enhanced values of $|\Gamma_B|$, implying large temperature changes in

[**] Besides lacking inversion symmetry, CuP has a two-fold rotation axis parallel to the *b*-axis which constrains the DM-vector **D** to lie within the *ac* plane. A finite DM interaction in CuP is consistent with the results of magnetic cooling experiments for two different orientations of the magnetic field with respect to **D**: the accessible lowest temperature T_f raises by about (10 ± 2) % for $B \parallel c$ as compared to $B \parallel b$.

[††] Using the distance between adjacent Cu ions, ranging from 6.357 Å to 8.908 Å, the dipole-dipole interaction energy is estimated to $J_{\mathrm{d\text{-}d}}/k_B \leq 0.012$ K.

response to small field variations, suggest that the system could be suitable for low-temperature magnetic refrigeration. To investigate its potential as a coolant, demagnetization experiments were carried out on CuP under near adiabatic conditions (see *SI Text III*) while simultaneously recording the sample temperature T_s (Fig. 2B). While the cooling process approaches an in-B linear behavior at higher temperature near (T_i, B_i) – such is seen in simple paramagnets where $T_s \propto B$ –, it becomes superlinear upon decreasing the temperature. This enhanced cooling effect, which is in accordance with the model calculations for the ideal system (broken lines in Fig. 2B), is a direct manifestation of quantum criticality. Upon further cooling, $T_s(B)$ passes through a rounded minimum, assigned T_0, for B close to B_s. The quantitative deviations from the theory curves, in particular an experimentally revealed T_0 staying clearly above the theoretically expected value, can be attributed only in part to non-ideal adiabatic conditions in the cooling experiments. Estimates of the effect of the parasitic heat flow onto the sample (see *SI Text V*) show that for an improved thermal isolation, T_0 can be reduced from 179 mK to about 132 mK (solid line in Fig. 2B). This implies that the main source for the deviations from the theoretical expectations lies in the presence of the above-mentioned perturbing interactions in CuP. The good agreement with the theory curves at higher temperatures, where these interactions are irrelevant, however, implies that for a better realization of the spin-½ AFHC, cooling to much lower temperatures should be possible.

In order to assess the principle limits of cooling near a QCP and its potential for applications, we compare some performance characteristics for the ideal spin-½ AFHC with those of two state-of-the-art adiabatic demagnetization refrigerator (ADR) materials (Fig. 3). These are $CrK(SO_4)_2 \cdot 12H_2O$ (chrome potassium alum CPA) and $FeNH_4(SO_4)_2 \cdot 12H_2O$ (ferric ammonium alum FAA), which cover the typical temperature range of applications for

paramagnetic salts and, due to their high efficiency, are also used in space applications (5-7). Representative parameters characterizing the performance of an ADR material include (i) the operating range, in particular its lower bound T_{min}. Standard ADR systems operate predominantly in a narrow temperature window near $T_{min} \approx$ 30-60 mK, while extensions down to only a few millikelvin are possible. Such low temperatures are otherwise accessible only by using elaborated ^{3}He-^{4}He dilution refrigerators, which, however, are much bigger compared to ADRs and cannot operate in a microgravity environment. Another important parameter is (ii) the "hold time" of the coolant, which is inversely proportional to its cooling power $\dot{Q}$. This quantity measures the ability of the refrigerant to absorb heat without warming up too rapidly. For some applications, (iii) the efficiency can be of importance. This includes the cooling capability per unit mass of refrigerant material and the ratio $\Delta Q_c/\Delta Q_m$. Here ΔQ_c is the heat the material can absorb after demagnetization to the final field B_f, and ΔQ_m the heat of magnetization released to a precooling stage held at a temperature T_i, the initial temperature of the magnetic cooling process. The efficiency can be an issue for modern multi-stage single-shot or continuous ADRs, such as the ones used in space (5), where the entire system has to be optimized with regard to precooling requirements and weight.

In principle, the cooling performance of a material is determined by the low-energy sector of its magnetic excitation spectrum, reflected in the low-temperature specific heat $C(T)$, and its variation with magnetic field. For paramagnetic salts, $C(T)$ at $B = 0$ is of Schottky type (see, e.g., ref. 40) due to an energy-level splitting arising from residual magnetic interactions. The resulting $C(T)$ maximum actually enables the material to be used as a coolant as it ensures a certain amount of cooling power during demagnetization at low temperatures. At the same time, the $1/T^2$-like decrement of the $C(T)$ anomaly at high temperatures and the accompanied

rapid reduction of the hold time (Fig. 3) constrain the operating range to a narrow temperature window around the position of the maximum. Thus, ADRs based on paramagnets are particularly well suited for applications within a narrow temperature range of operation.

This is different for the spin-½ AFHC near B_s: due to its peculiar excitation spectrum (35), i.e. the abundance of low-energy excitations above the QCP, (in principle) arbitrarily small values of T_{min} can be reached, while keeping the cooling power large. At the same time, due to the extraordinarily large specific heat above the QCP, with a peak centered at a temperature around $J/2k_B$ (Fig. 1), the system affords extended hold times also for temperatures largely exceeding the maximum position (Fig. 3). Thus, materials near a B-induced QCP can be an excellent alternative to paramagnets for those applications where the temperature has to be varied over an extended range. This includes the possibility to reach very low temperatures, albeit with reduced hold times. In addition, the present quantum critical system, despite its low spin value, can absorb an amount of energy ΔQ_c which is almost comparable to that of the spin-3/2 (CPA) and spin-5/2 (FAA) paramagnets (Fig. 4). The quantum critical system excels, however, by its high efficiency $\Delta Q_c/\Delta Q_m$, which exceeds the corresponding numbers for the paramagnets by a factor 2-3 (Fig. 4). This is due to the system's ability to absorb energy even at temperatures as high as T_i, in contrast to the paramagnets, where the absorption essentially occurs at low temperatures $T < T_i$ (Fig. 4). Besides these performance characteristics, the applicability of a material as a coolant may also depend on other material-specific features such as its thermal conductivity and the possibility to realize a good thermal contact to the body to be cooled. In terms of heat transport, the spin-½ AFHC near the B-induced QCP is particularly favorable as it shows a comparatively large spin thermal conductivity along the spin chains, which even dominates the material's thermal transport at low temperatures, see,

e.g. ref. 42. In contrast, a small thermal conductivity and a weak thermal contact between the coolant and another body are principal concerns for paramagnetic ADR materials (40). Here, problems can arise due to the extreme hydration of these materials, required to reduce the mutual interactions between the magnetic centers, and the materials' sensitivity to decompose if water is allowed to evaporate through imperfections in the materials' housing.

Conclusions and outlook

We have demonstrated that the strong enhancement of the magnetocaloric effect, arising from quantum fluctuations near a *B*-induced quantum-critical point, can be used for realizing an efficient and flexible magnetic cooling with a good cooling performance over an extended range of temperatures. While the spin-½ AFHC, thanks to its simplicity, has enabled the provision of a proof-of-principle demonstration, extensions of this concept are obvious and may guide the search for materials with further improved cooling performance. On the one hand, this includes low-dimensional spin systems with geometric frustration, such as the saw-tooth chain discussed in ref. 30. In contrast to the uniform spin-½ AFHC discussed here, where the enhanced MCE results from large relative changes of the entropy across B_s, while S vanishes for $T \rightarrow 0$, certain geometrically frustrated spin configurations in one dimension support a significant zero-temperature entropy (43). As a consequence, in these systems there is a large absolute variation of entropy across B_s and hence a large $\partial T/\partial B$ down to, in principle, arbitrarily low temperatures, limited by weak residual interactions, such as dipole-dipole interactions. Consequently, a further enhancement of the MCE can be expected for those frustrated magnetic systems. The combination of quantum criticality with (i) low dimensionality, assuring a high density of low-energy excitations, and (ii) geometric

frustration, opens up a promising route to search for materials with further enhanced MCE. Of particular interest are highly symmetric (yet low-dimensional) spin systems with gapped ground states in zero field and *B*-inducd XY antiferromagnetic states, since the high symmetry in spin space prevents the system from developing *B*-induced gaps. Likewise, as a large spin entropy can cause a large thermopower in conducting materials (44), conducting magnets driven close to a field-induced QCP would be a very interesting class of materials for the search for thermoelectric (Peltier) cooling systems with high efficiency. Finally, the concept of using quantum criticality for magnetic cooling might also be applicable to cold atom experiments and help there to realize low-temperature magnetic and superfluid phases.

Materials and methods

The specific heat was measured as a function of temperature by employing a compensated heat-pulse technique in combination with a ^{3}He-^{4}He dilution refrigerator (see *SI Text I*). For the magnetic susceptibility measurements a state-of-the-art compensated-coil ac-susceptometer adapted to a top-loading ^{3}He-^{4}He dilution refrigerator was used (see *SI Text I*). The MCE was determined by employing a specially-designed calorimeter (see *SI Text III*). For

the magnetic cooling experiments, the setup was modified to ensure quasi-adiabatic conditions (see *SI Text IV*).

Acknowledgments

A. H. acknowledges financial support by the Deutsche Forschungsgemeinschaft (DFG) via a Heisenberg fellowship. Work at Goethe-University Frankfurt was supported by the DFG in the consortium SFB/TR49.

References

[1] Lounasmaa O V (1974) *Experimental Principles And Methods Below 1 K*. (Academic Press, New York).

[2] Tegus O, Brück E, Buschow KHJ, de Boer FJ (2002) Transition-metal-based magnetic refrigerants for room-temperature application. *Nature* 415: 150-152.

[3] Tishin AM, Spichkin I (2003) *The Magnetocaloric Effect And Its Applications* (Institue of Physics Publishing, Bristol).

[4] Gschneidner Jr. KA, Pecharsky VK, Tsokol AO (2005) Recent developments in magnetocaloric materials. *Rep Prog Phys* 68:1479-1539.

[5] Shirron PJ (2007) Cooling capabilities of adiabatic demagnetization refrigerators. *J Low Temp Phys* 148:915-920.

[6] Hagmann C, Richards PL (1995) Adiabatic demagnetization refrigerators for small laboratory experiments and space astronomy. *Cryogenics* 35:303-309.

[7] Porter F S, et al. (1999) The detector assembly and the ultra low temperature refrigerator for XRS. Proc SPIE 3765:729-740.

[8] Jaime M, Kim KH, Jorge G, McCall S, Mydosh JA (2002) High magnetic field studies of the hidden order transition in URu_2Si_2. *Phys Rev Lett* 89:287201.

[9] Zapf VS, et al. (2006) Bose-Einstein condensation of S=1 Nickel spin degrees of freedom in $NiCl_2$-4SC$(NH_2)_2$. *Phys Rev Lett* 96:077204.

[10] Rost AW, et al. (2009) Entropy landscape of phase formation associated with quantum criticality in $Sr_3Ru_2O_7$. *Science* 325:1360-1363.

[11] Aczel AA, et al. (2009) Field-induced Bose-Einstein condensation of triplons up to 8 K in $Sr_3Cr_2O_8$. *Phys Rev Lett* 103:207203.

[12] Aczel AA, et al. (2009) Bose-Einstein condensation of triplons in $Ba_3Cr_2O_8$. *Phys Rev B* 79:100409(R).

[13] Lang M, et al. (2010) Large magnetocaloric effect at the saturation field of an S=1/2 antiferromagnetic Heisenberg chain. *J Low Temp Phys* 159:88-91.

[14] Tokiwa Y, et al. (2009) Divergence of the magnetic Grüneisen ratio at the field-induced quantum critical point in $YbRh_2Si_2$. *Phys Rev Lett* 102:066401.

[15] Bianchi A, et al. (2002) First-order superconducting phase transition in $CeCoIn_5$. *Phys Rev Lett* 89:137002.

[16] Jaime M, et al. (2004) Magnetic-field-induced condensation of triplons in Han Purple pigment $BaCuSi_2O_6$. *Phys Rev Lett* 93:087203.

[17] Silhanek AV, et al. (2006) Irreversible dynamics of the phase boundary in $U(Ru_{0.96}Rh_{0.4})_2Si_2$ and implications for ordering. *Phys Rev Lett* 96:136403.

[18] Fortune NA, et al. (2009) Cascade of magnetic-field-induced quantum phase transitions in a spin-1/2 triangular-lattice antiferromagnet. *Phys Rev Lett* 102:257201.

[19] Samulon, et al. (2009) Asymmetric quintuplet condensation in the frustrated S = 1 spin dimer compound $Ba_3Mn_2O_8$. *Phys Rev Lett* 103:047202.

[20] Sachdev S (1999) *Quantum Phase Transitions* (Cambridge University Press, Cambridge, England).

[21] Löhneysen Hv, Rosch A, Vojta M, Wölfle P (2007) Fermi-liquid instabilities at magnetic quantum phase transitions. *Rev Mod Phys* 79:1015-1076.

[22] Gegenwart P, Si Q, Steglich F (2008) Quantum criticality in heavy-fermion metals. *Nat Phys* 4:186-197.

[23] Bitko D, Rosenbaum TF, Aeppli G (1996) Quantum critical behavior for a model magnet. *Phys Rev Lett* 77:940-943.

[24] Lake B, Tennant DA, Frost CD, Nagler SE (2005) Quantum criticality and universal scaling of a quantum antiferromagnet. *Nat Mat* 4:329-334.

[25] Mathur N, et al. (1998) Magnetically mediated superconductivity in heavy fermion compounds. *Nature* 394:39-43.

[26] Pfleiderer C, Reznick D, Pintschovius L, Löhneysen Hv, Garst M, Rosch A (2004) Partial order in the non-fermi liquid phase of MnSi. *Nature* 427:227-231.

[27] Zhu L, Garst M, Rosch A, Si Q (2003) Universally diverging Grüneisen parameter and the magnetocaloric effect close to quantum critical points. *Phys Rev Lett* 91:066404.

[28] Garst M, Rosch A (2005) Sign change of the Grüneisen parameter and magnetocaloric effect near quantum critical points. *Phys Rev B* 72:205129.

[29] Küchler R, et al. (2003) Divergence of the Grüneisen ratio at quantum critical points in heavy-fermion metals. *Phys Rev Lett* 91:066405.

[30] Zhitomirsky ME, Honecker A (2004) Magnetocaloric effect in one-dimensional antiferromagnets. *J Stat Mech: Theor Exp* P07012.

[31] Bonner JC, Nagle JF (1972) Comment on magnetic cooling of solid He^3. *Phys Rev A* 5:2293-2296.

[32] Stone MB, et al. (2003) Extended quantum critical phase in a magnetized spin-1/2 antiferromagnetic chain. *Phys Rev Lett* 91:037205 (2003).

[33] Castillo O, Lugue A, Sertucha J, Román P, Lloret F (2000) Synthesis, crystal structure, and magnetic properties of a one-dimensional polymeric copper(II) complex containing an unusual 1,1′-bicoordinated oxalato bridge. *Inorg Chem* 39:6142-6144.

[34] Prokofiev A V, Assmus W, Remović-Langer K, Pashchenko P, Tsui Y, Wolf B, Lang M (2007) Crystal growth and magnetic properties of the copper coordination polymer $[Cu(\mu\text{-}C_2O_4)(4\text{-aminopyridine})_2(H_2O)]_n$. *Cryst Res Technol* 42:394-399.

[35] Klümper A (1998) The spin-1/2 Heisenberg chain: thermodynamics, quantum criticality and spin-Peierls exponents. *Eur Phys J B* 5:677-685.

[36] Hammar PR, et al. (1999) Characterization of a quasi-one-dimensional spin-1/2 magnet which is gapless and paramagnetic for $g\mu_B H \leq J$ and $k_B T \ll J$. *Phys Rev B* 59:1008-1015.

[37] Trippe C, Honecker A, Klümper A, Ohanyan V (2010) Exact calculation of the magnetocaloric effect in the spin-1/2 XXZ-chain. *Phys Rev B* 81:054402.

[38] Oshikawa M, Affleck I (1997) Field-induced gap in S = ½ antiferromagnetic chains. *Phys Rev Lett* 79:2883-2886.

[39] Capraro F, Gros C (2002) The spin-1/2 anisotropic Heisenberg chain in longitudinal and transversal magnetic fields: a DMRG study. *Eur Phys J B* 29:35-40.

[40] Vilches O E, Wheatley J C (1966) Measurements of the specific heat of three magnetic salts at low temperatures. *Phys Rev* 148:509-516.

[41] Pobell F (1992) *Matter And Methods At Low Temperatures*. (Springer Berlin Heidelberg New York).

[42] Sologubenko AV, et al. (2007) Magnetothermal transport in the spin-1/2 chain of Copper Pyrazin Dinatrate. *Phys Rev Lett* 98:107201.

[43] Derzhko O, Richter J, Honecker H, Schmidt H-J (2007) Universal properties of highly frustrated quantum magnets in strong magnetic fields. *Low Temp Phys* 33:745-756.

[44] Wang Y, Rogado N S, Cava R J, Ong N P (2003) Spin entropy as the likely source of enhanced thermopower in $Na_xCo_2O_4$. *Nature* 423:425-428.

Figure Legends

Fig. 1. **(A)** Specific heat $C_B(T)$ measured in a constant magnetic field of B = 0.15 T (red symbols) and 7.14 T (green symbols). While the data at B = 0.15 T « B_s (saturation field) are characterized by an in-T linear contribution $C/T \propto J^{-1}$ for T « J/k_B (35), those at B = 7.14 T > B_s show an activated behavior, reflecting the opening of an excitation gap in the field-induced ferromagnetic state. The red solid line is the result of Bethe Ansatz calculations (BAC) (35) for a spin-½ AFHC with J/k_B = 3.2 K, g = 2.087, B/B_s = 0.0329, representing the magnetic contribution C_{mag}, in addition to a small phonon contribution $C_{ph} = \beta \cdot T^3$ (black solid line). The coefficient β, the only adjustable parameter, was determined from a least-squares fit of $C = C_{ph} + C_{mag}$ to the experimental data taken at B = 0.15 T. The green solid line corresponds to $C_{ph} + C_{mag}$, with C_{mag} obtained from BAC for B/B_s = 1.564, corresponding to B = 7.14 T. The excellent agreement of the $C_B(T)$ data with the model calculations at small fields and the moderate deviations at 7.14 T indicate the presence of additional field-dependent terms in the material's Hamiltonian which become relevant at high fields. **(B)** Blue open circles represent the magnetic susceptibility $\chi = \partial M/\partial B$, taken on single-crystalline material immersed in the ^{3}He-^{4}He mixture kept at a constant temperature T = 0.055 K with $B \parallel b$-axis. The field was swept at a low rate of 0.1 T/min, ensuring constant-temperature conditions. The growth of χ upon increasing the field, the sharp peak at 4.09 T and the disappearance of χ at higher fields reflect the transition from the antiferromagnetic ($B < B_s$) to the polarized ferromagnetic state ($B > B_s$) at B_s = 4.09 T. The solid line represents a parameter-free description of the data based on the above-mentioned BAC for J/k_B = 3.2 K and g = 2.33 (34).

Fig. 2. (A) Variation of Γ_B, approximated by $\Gamma_B \approx T^{-1} \cdot (\Delta T/\Delta B)_{S \approx \text{const}}$ (see *SI Text IV*), with field at T = 0.32 K (blue squares) and 0.97 K (black triangles) for $B \parallel b$-axis. For Γ_B data at an intermediate temperature T = 0.47 K, see ref. 13. Solid lines are the results of Quantum-Monte-Carlo (QMC) simulations and exact diagonalization of a finite-size lattice of the spin-½ AFHC for the corresponding temperatures (same color code) by using J/k_B = 3.2 K. A g value of 2.28 has been used in the calculations to account for a small misalignment of the crystals. Error bars (below symbol size for the data taken at 0.97 K) of experimental data correspond to statistical error. The systematic error, mainly originating from the internal time constant of the resistance bridge in combination with the sweep time applied, is estimated to be of the order of 1 %. **(B)** Sample temperature (symbols) measured by demagnetizing a collection of CuP single crystals ($B \parallel b$-axis) of total mass of 25.23 mg under near adiabatic conditions (see *SI Text III*). The initial parameters were set to B_i = 7 T and T_i = 1.40 K (green symbols) and 1.21 K (red symbols). The field was swept with a rate $\Delta B/\Delta t$ = -0.3 T/min for $B \geq 6$ T and -0.5 T/min for $B < 6$ T. The red solid line represents the experimental data (for T_i = 1.21 K) corrected for the effect of a parasitic heat flow (see *SI Text V*). Broken lines are those ideal isentropes, derived from the exact result for the entropy of the spin-½ AFHC (37), which correspond to the same initial conditions (B_i, T_i). The **insert in (B)** shows the temperature dependence of Γ_B, approximated by $\Gamma_B \approx T^{-1} \cdot (\Delta T/\Delta B)_{S \approx \text{const}}$ (see *SI Text IV*), at constant fields below (B = 3.5 and

4.0 T) and above (4.3 T) B_s. The deviations of the experimental data from the model calculations for the ideal system (solid lines, same color code as used for the experimental data) grow with decreasing the temperature. The data reveal an anomaly around 0.22 K, the position of which shows no significant field dependence within the field range investigated. This feature is likely to be related to the opening of a field-induced gap in the magnetic excitation spectrum.

Fig. 3. Increase of the sample temperature T_s with time after demagnetization to $B = B_f$ calculated for a heat load of 5 μW applied under adiabatic conditions to 100 gram substance of a spin-1/2 AFHC with J/k_B = 3.2 K (red solid line), a spin-3/2 ($CrK(SO_4)_2 \cdot 12H_2O$ in short CPA) (magenta solid line) and a spin-5/2 ($Fe(NH_4)(SO_4)_2 \cdot 12H_2O$ in short FAA) (blue solid line) paramagnetic salt (see *SI Text VI*). For the paramagnets at $B_f = 0$, base temperatures of $T_{min} \approx$ 0.01-0.015 K (CPA) and ≈ 0.04-0.05 K (FAA) can be reached, which lie close to the transition temperature to long-range antiferromagnetic order at T_N = 0.01 K (CPA) and 0.04 K (FAA). In contrast, for the spin-1/2 AFHC, cooling to an (in principle) arbitrarily small T_{min} is possible. In practice, however, a finite T_{min} will result from the presence of small perturbing interactions such as weak inter-chain couplings, dipole-dipole interactions or single-ion anisotropies. The calculations for T_s(time) are based on computed (spin-1/2 AFHC) and measured (CPA and FAA) (40) specific heat data. The paramagnets exhibit long hold times only in a narrow temperature range around T_{min}, defined by the position of their Schottky-type $C(T,B=0)$ maximum. For temperatures somewhat above T_{min}, T_s rapidly increases with exposure time t, approximately as t^2 for FAA. This contrasts with the spin-1/2 AFHC, where T_s increases only moderately with time as $t^{2/3}$. A further flattening of $T_s(t)$, at not too low temperatures, can be achieved for $B_f < B_s$; see, e.g. the warming curve for $B_f = 0.75B_s$ (broken orange line). Crossing B_s upon demagnetization from (B_i, T_i) = (7 T, 1.3 K) is, however, accompanied by a moderate warming to $T_{min} \approx$ 0.112 K.

Fig. 4. Calculated molar magnetic entropy $S_{mag}(T, B=\text{const.})$ as a function of temperature of the spin-1/2 AFHC with J/k_B = 3.2 K for an initial field of B_i = 7.14 T (red broken line) and a final field $B_f = B_s$ = 4.09 T (red solid line). For comparison, $S_{mag}(T, B=\text{const.})$ of the spin-5/2 paramagnetic salt $Fe(NH_4)(SO_4)_2 \cdot 12H_2O$ is shown for B_i = 2 T (blue broken line) and B_f = 0 (blue solid line); the data were taken from refs. 40 and 41. In the cooling process, the materials are first isothermally magnetized (path AB for example), and then, after thermal isolation, adiabatically demagnetized (path BC) to the final temperature T_f. For T_i = 1.3 K, for example, adiabatic demagnetization from 7.14 T to 4.09 T for the spin-1/2 AFHC results in T_f = 0.021 K, while demagnetization from 2 T to zero field for the spin-5/2 paramagnet leads to T_f = 0.026 K. The systems warm up along their entropy curves at the final demagnetization field $S_{mag}(T, B=B_f)$. The heat of magnetization at $T = T_i$, $\Delta Q_m = T_i \cdot [S_{mag}(B_f, T_i) - S_{mag}(B_i, T_i)]$, and the heat that the material is able to absorb after adiabatic

demagnetization, $\Delta Q_c = \int_{T_f}^{\infty} T \cdot (\partial S_{mag} / \partial T)_{B_f} \, dT$, can be read off the figure. For the spin-5/2 paramagnet (PM) $Fe(NH_4)(SO_4)_2 \cdot 12H_2O$, for example, ΔQ_m = 14.3 J/mole is given by the area of the rectangle ABDE, while ΔQ_c = 1.22 J/mole corresponds to the hatched area in that rectangle. The efficiency factor $\Delta Q_c/\Delta Q_m$ in the temperature range indicated amounts to 26 % for the spin-1/2 AFHC as compared to only 9 % for the spin-5/2 paramagnet. For the spin-3/2 system $CrK(SO_4)_2 \cdot 12H_2O$ (see *SI Text VII*) one finds ΔQ_m = 10.01 J/mole, ΔQ_c = 1.06 J/mole and $\Delta Q_c/\Delta Q_m$ of 11 %.

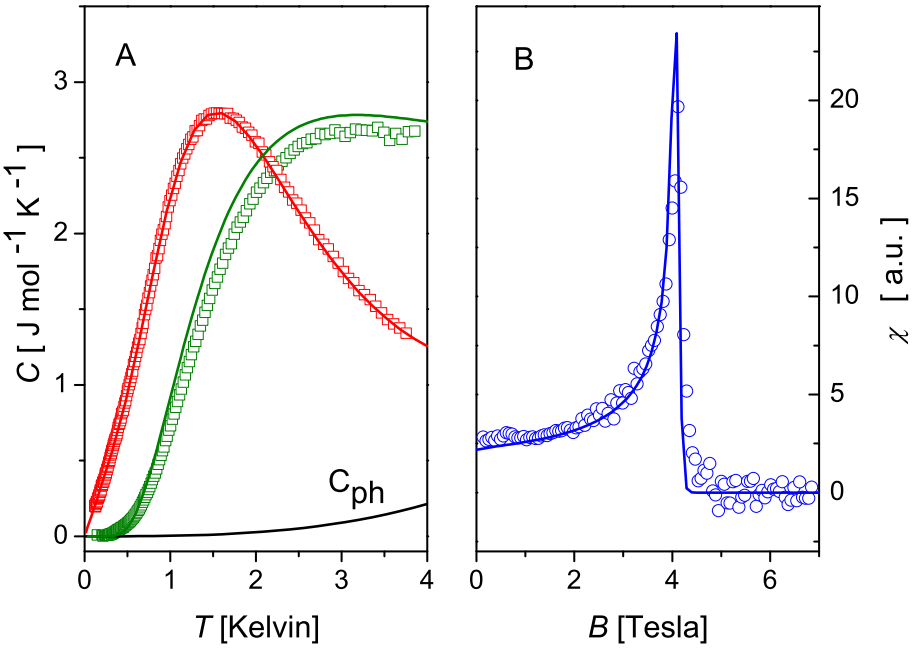

Figure 1

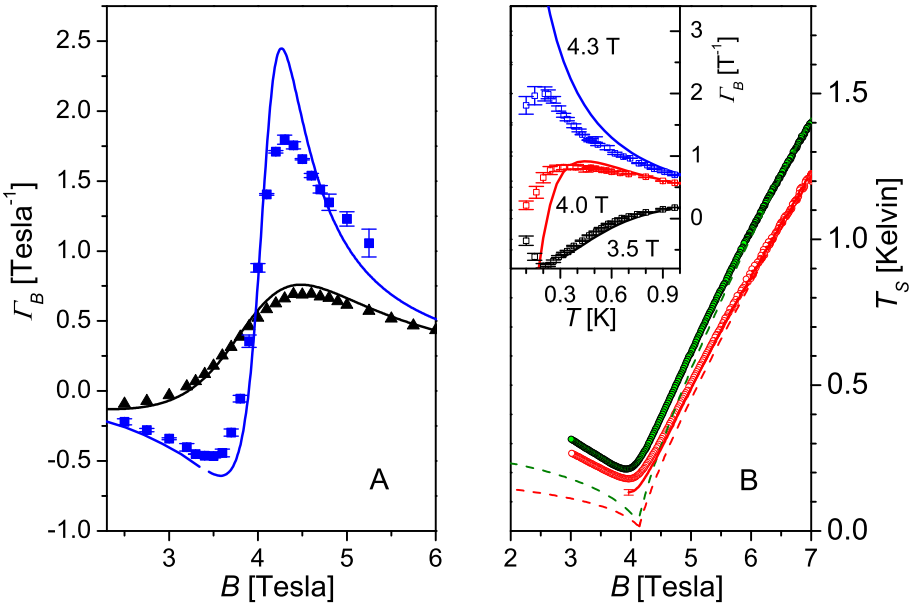

Figure 2

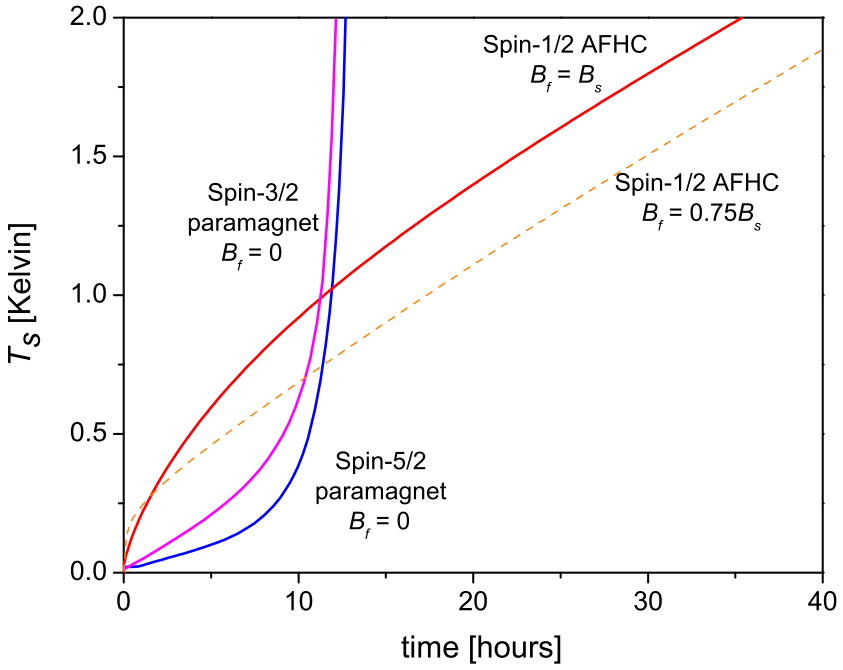

Figure 3

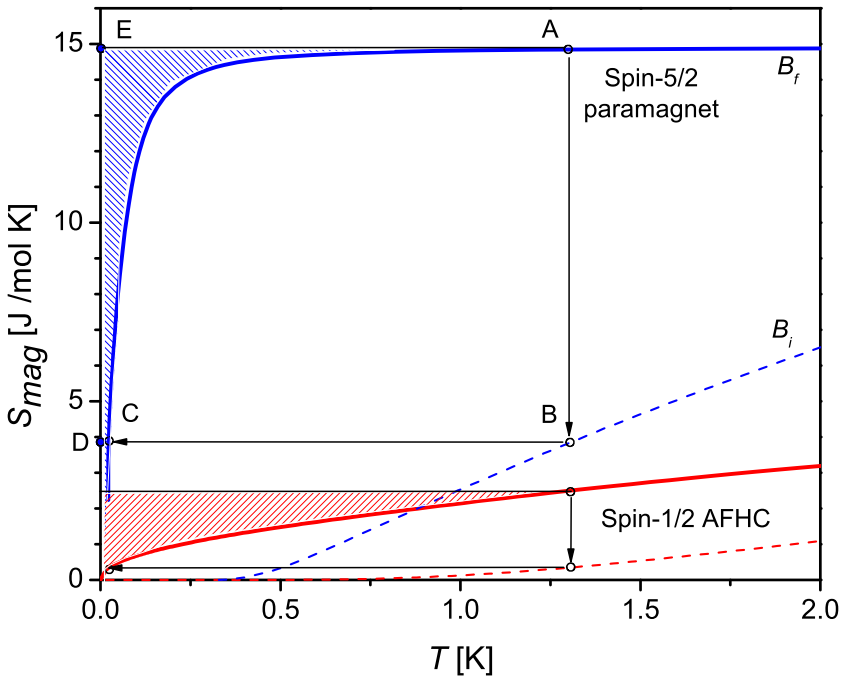

Figure 4

Supporting Information for "Magnetocaloric effect and magnetic cooling near a field-induced quantum-critical point"

Bernd Wolf[a,1], Yeekin Tsui[a,2], Deepshikha Jaiswal-Nagar[a], Ulrich Tutsch[a], Andreas Honecker[b], Katarina Remović-Langer[a], Georg Hofmann[a], Andrei Prokofiev[c], Wolf Assmus[a], Guido Donath[d], and Michael Lang[a]

[a]Physics Institute, Goethe-University, Max-von-Laue Strasse 1, 60438 Frankfurt(M), Germany;

[b]Institute for Theoretical Physics, Georg-August-University Göttingen, Friedrich-Hund-Platz 1, 37077 Göttingen, Germany;

[c]Institute of Solid State Physics, Vienna University of Technology, Wiedner Hauptstrasse 8-10, 1040 Vienna, Austria;

[d]Max-Planck-Institut for Chemical Physics of Solids, Nöthnitzer Strasse 40, 01187 Dresden, Germany;

[1]To whom correspondence may be addressed. E-mail: wolf@physik.uni-frankfurt.de

[2]Present address: Department of Physics, Durham University, United Kingdom

I. Sample characterization. Single crystalline samples of CuP have been characterized by specific heat and magnetic susceptibility measurements. The specific heat was measured as a function of temperature for 0.1 K ≤ T ≤ 4 K at varying magnetic fields by employing a compensated heat-pulse technique (1) in combination with a ^{3}He-^{4}He dilution refrigerator. The specific-heat sample was composed of several single crystals with a total mass of 36.3 mg, the *ac*–planes of which were aligned parallel to the magnetic field. The magnetic susceptibility was measured on a single crystal of CuP down to T = 0.055 K and magnetic fields up to 8.5 T by using a state-of-the-art compensated-coil ac-susceptometer adapted to a top-loading ^{3}He-^{4}He dilution refrigerator. The crystal was oriented with its *b*-axis running parallel to the applied magnetic field. Empty-coil measurements were performed to determine the magnetic background.

II. Model calculations. The spin-1/2 antiferromagnetic Heisenberg chain is exactly solvable, and, indeed, we used those exact results for calculating the specific heat (2), magnetic susceptibility (2), and entropy (3). The theory curves shown in Fig. 2(A) in the main text are based on exact diagonalization and Quantum-Monte-Carlo simulations which are essentially exact (see ref. (3) for details). Finally, in some cases we have used exact diagonalization for the spin-1/2 antiferromagnetic-Heisenberg-chain model with 20 sites, as outlined in ref. 4.

III. The calorimeter – design features. The MCE was measured by attaching several single crystals with a total mass of 7.23 mg to a specially-designed calorimeter (see below) by applying a small amount of Apiezon N-grease. For the magnetic cooling experiments, where field sweeps from B_i = 7 T to B_f = 3 T were carried out with a rate of 0.3 – 0.5 T/min, the setup was modified in the following way to ensure quasi-adiabatic conditions: single crystals of total mass of about 25 mg were used and the thermal coupling between the calorimeter and the thermal bath was reduced by a factor 3-9, depending on the temperature.

The calorimeter for measuring the MCE consists of a sapphire plate (5×5×0.3 mm^3) and a grinded RuO_2 resistor, which serves as a thermometer. The heat capacity of the calorimeter,

amounting to less than 10^{-4} of that of the composite CuP sample over the whole field ($B < 7.2$ T) and temperature ($T \leq 2$ K) range investigated, can be neglected in the measurements of the MCE. Four thin Pt-W wires (25 μm in diameter and ~ 1.5 cm in length) were used to make electrical contacts to the thermometer. The calorimeter was suspended by two thin nylon strings, each 0.1 mm in diameter. The crystals were oriented such that the external magnetic field was parallel to the *b*-axis. The thermal conductance κ_{cal} between the calorimeter and the surrounding thermal bath was determined from the MCE experiment through $\kappa_{cal} = C/\tau$. Here C is the specific heat of the sample, determined independently, and τ the relaxation time by which the sample temperature relaxes back to the bath temperature T_b after a field change ΔB. These measurements yield $\kappa_{cal} \approx 2.5 \cdot 10^{-8}$ W/K at 0.32 K and $1.1 \cdot 10^{-7}$ W/K at 0.9 K. The relaxation time τ varies from about 1500 s (at low temperatures and small fields) to about 90 s (for higher temperatures and large fields).

IV. Quasi-adiabatic (step-like) measurements of the magnetocaloric effect. To reduce systematic errors in the data analysis, which may result from a too fast relaxation, see below, the measurements of the MCE were restricted to fields $B \leq 6$ T and $T \leq 1$ K, where $\tau \geq 300$ s. In this range of parameters, the MCE was determined by employing a step-like technique which ensures quasi-adiabatic conditions (for a setup operating in the opposite limit, i.e. under highly non-adiabatic conditions, see ref. 5): at a fixed bath temperature T_b, and the calorimeter initially in thermal equilibrium with the bath, the magnetic field was swept in a small step ΔB while simultaneously measuring the changes in the sample temperature T_s. The latter was detected with an ac-resistance bridge with a resolution of $\Delta R/R \sim 10^{-5}$ and an internal time constant of ~ 0.3 – 0.4 s, depending on the temperature range. T_b during the field sweeps was stabilized within ± 0.025 mK. The temperature of the calorimeter, prior to a field sweep, varies typically by ± 0.04 mK. A field change of $\Delta B = 20$ mT was applied to ensure measurable temperature changes ΔT_s. The time for sweeping the field was kept at $t_{swp} \sim 65$ s, which is short enough to guarantee quasi-adiabatic conditions for relaxation times 300 s $\leq \tau \leq 1500$ s, while keeping effects due to finite internal time constants and eddy-current heating in the metallic parts of the calorimeter small. The latter effect was eliminated by using two

consecutive sweeps, an up sweep by ΔB, followed by a down sweep by $-\Delta B$, and estimating $\Delta T_s = \Delta T_{+\Delta B} - \Delta T_{-\Delta B}$ (Fig. S1A). After each field change, T_s relaxes back to T_b. This process can be well described by a single exponential $T_s \propto \exp(-t/\tau)$, except for $t \ll \tau$, indicating that all internal time constants τ_i, corresponding to the thermal couplings of the sample to the calorimeter and the calorimeter to the thermometer, are much smaller than τ. Occasional weak thermal drifts of the bath or the calorimeter, with $\Delta T_{drift} \ll \Delta T_s$, were accounted for by subtracting a small in-t linear background from $T_s(t)$. To extract the temperature changes $\Delta T_{+\Delta B}$ and $\Delta T_{-\Delta B}$ from the data, an "equal-areas" construction was employed, whereby the gradual changes in T_s throughout the field changes were replaced by idealized sharp ones (Fig. S1B). This procedure also compensates, to a good approximation, for uncertainties resulting from the internal time constants τ_i.

V. Corrections for non-adiabaticity in the demagnetization experiments. The magnetic cooling experiments on CuP were performed under quasi-adiabatic conditions using the same calorimeter as employed for measuring the MCE but with a reduced thermal coupling between calorimeter and thermal bath. Even under these improved conditions, the finite heat flow dQ/dt on the calorimenter (due to the wiring, measuring current and a finite pressure of residual gas) gives rise to a parasitic temperature drift $\dot{T}_{para}$. Thus, at a given time t_0 (which corresponds to a magnetic field B), the experimentally determined sample temperature $T_{exp}(B, t_0)$ has to be corrected by

$$T_{corr}(B,t_0) = T_{exp}(B,t_0) - \int_0^{t_0} \dot{T}_{para}\, dt, \qquad \text{(S1)}$$

This correction procedure is applicable only for a sufficiently weak parasitic heat flow, which does not strongly affect the whole demagnetization process, see, e.g. ref. 6. The parasitic temperature drift is given by

$$\dot{T}_{para} = \frac{\dot{Q}_{para}(B,t)}{C(B,t)}, \qquad \text{(S2)}$$

where $\dot{Q}(B(t),T(t))$ is the parasitic heat flow and $C(B(t),T(t))$ the specific heat at a magnetic field and a temperature corresponding to the time t. The heat flow $\dot{Q}$ is given by $\dot{Q} = \kappa \cdot \Delta T$, where ΔT is the temperature gradient between the bath and the calorimeter and κ denotes the thermal conductance between calorimeter and bath. The quantity $\kappa(T)$ was determined from relaxation experiments at various temperatures and fields. The error bar of the so-derived $\kappa(T)$-values amounts to approximately ± 15% for temperatures 0.250 K ≤ T ≤ 2.01 K. In this temperature range, $\kappa(T)$ varies, to a good approximation, linear in temperature. For the determination of $C(B, t)$ in eq. S2, specific heat data on CuP, measured as a function of temperature at various fixed fields up to 7.14 T, were used to determine the specific heat landscape in the relevant field and temperature range. The quantity $C(B, t)$ was then obtained by parameterization, using a 4^{th}-order polynomial, of the data along the $(B(t), T(t))$ trajectory the sample took during the demagnetization experiment. After having transformed the variables T and B into time by using appropriate inverse functions, the numerical integration in eq. (S1) was carried out. For the demagnetization experiment starting at T_i = 1.25 K (= T_b) and B_i = 7 T, for example, a minimal temperature of T_0 = 179 mK was obtained at a field of B_f = 3.97 T. According to the above procedure, this value has to be corrected to T_0 = (132 ± 9) mK for idealized adiabatic conditions.

VI. Calculations of the warming rate under an external heat load for $CrK(SO_4)_2 \cdot 12H_2O$ and $Fe(NH_4)(SO_4)_2 \cdot 12H_2O$ – two standard magnetic coolants. The time evolution of a material's temperature under adiabatic conditions and exposed to a given heat load P is obtained from the internal energy $U(T)$, derived by integrating $C(T)$ and the equation $dU(T(t))/dt = P$. Integration then leads to $U(T(t_i)) - U(T(t)) = (t_i - t) \cdot P$. The paramagnetic salts $CrK(SO_4)_2 \cdot 12H_2O$ (CPA) and $Fe(NH_4)(SO_4)_2 \cdot 12H_2O$ (FAA), containing Cr^{3+} ions with spin 3/2 and Fe^{3+} ions with spin 5/2, respectively, represent state-of-the-art coolants for low-temperature magnetic refrigeration, including space applications (see, e.g., refs. 7, 8, 9). The salts exhibit long-range antiferromagnetic order below 10 mK (CPA) and 40 mK (FAA),

which sets a lower bound to the accessible base temperature T_{min}. For calculating the materials' warming rate at $B_f = 0$, the specific heat data $C(T)$ reported in ref. 10 were used.

VII. Adiabatic demagnetization of the paramagnetic salt $CrK(SO_4)_2 \cdot 12H_2O$. In the cooling process, the materials are first isothermally magnetized (path AB), and then, after thermal isolation, adiabatically demagnetized (path BC) to the final temperature T_f. For T_i = 1.3 K and B_i = 2 T, for example, for the spin-3/2 paramagnet reaches T_f = 0.010 K. The system warms up along its entropy curve at the final demagnetization field $S_{mag}(T, B=B_f)$. The heat of magnetization at $T = T_i$, $\Delta Q_m = T_i \cdot [S_{mag}(B_f, T_i) - S_{mag}(B_i, T_i)]$, and the heat that the material is able to absorb after adiabatic demagnetization, $\Delta Q_c = \int_{T_f}^{\infty} T \cdot (\partial S_{mag} / \partial T)_{B_f} \, dT$, can be read off figure S2. For the spin-3/2 paramagnet $Cr(NH_4)(SO_4)_2 \cdot 12H_2O$, we obtain ΔQ_m = 10.1 J/mole, corresponding to the area of the rectangle ABDE, and ΔQ_c = 1.06 J/mole, corresponding to the hatched area in that rectangle. This results in an efficiency factor $\Delta Q_c / \Delta Q_m$ in the temperature range indicated of about 11 %.

References

1 Wilhelm H, Lühmann T, Rus T, Steglich F (2004) A compensated heat-pulse calorimeter for low temperatures. *Rev Sci Instrum* 75:2700-2705.

2 Klümper A (1998) The spin-1/2 Heisenberg chain: thermodynamics, quantum criticality and spin-Peierls exponents. *Eur Phys J B* 5:677-687.

3 Trippe C, Honecker A, Klümper A, Ohanyan V (2010) Exact calculation of the magnetocaloric effect in the spin-1/2 XXZ-chain. *Phys Rev B* 81:054402.

4 Zhitomirsky ME, Honecker A (2004) Magnetocaloric effect in one-dimensional antiferromagnets. *J Stat Mech: Theor Exp* P07012.

5 Rost AW, et al. (2009) Entropy landscape of phase formation associated with quantum criticality in $Sr_3Ru_2O_7$. *Science* 325:1360-1363.

6 Sosin S S, et al. (2005) Magnetocaloric effect in pyrochlore antiferromagnet $Gd_2Ti_2O_7$. *Phys Rev B* 71:094413.

7 Hagmann C, Richards PL (1995) Adiabatic demagnetization refrigerators for small laboratory experiments and space astronomy. *Cryogenics* 35:303-309.

8 Porter F S, et al. (1999) The detector assembly and the ultra low temperature refrigerator for XRS. Proc SPIE 3765:729-740.

9 Shirron PJ (2007) Cooling capabilities of adiabatic demagnetization refrigerators. *J Low Temp Phys* 148:915-920.

10 Vilches O E, Wheatley J C (1966) Measurements of the specific heat of three magnetic salts at low temperatures. *Phys Rev* 148:509-516.

11 Pobell F (1992) *Matter And Methods At Low Temperatures*. (Springer Berlin Heidelberg New York).

Figure Legends

Fig. S1. (A) Exemplary illustration of the measuring cycle for the determination of the MCE at $T \cong 0.324$ K and $B = 4.3$ T: Time dependence of the sample temperature T_s (black spheres), initially in equilibrium with the bath temperature $T_b \approx 0.324$ K and at an external field of $B = 4.29$ T, in response to an up and subsequent down sweep of the magnetic field (red solid line) by $\Delta B = 20$ mT using a sweep rate of 0.31 mT/s. **(B)** Change of sample temperature $\Delta T_s = T_s - T_b$ around the time of the field sweep with duration t_{swp}. Red solid line corresponds to an exponential fit $T_s \propto \exp(-t/\tau)$ with $\tau = 603$ s, performed over a time period of typically 3 – 4 times τ. The blue vertical arrow, corresponding to $\Delta T_{+\Delta B}$, is derived from an "equal-areas" construction, as indicated in the figure.

Fig. S2. Calculated molar magnetic entropy $S_{mag}(T, B=\text{const.})$ of the spin-3/2 paramagnetic salt $Cr(NH_4)(SO_4)_2 \cdot 12H_2O$ shown for $B_i = 2$ T (orange broken line) and $B_f = 0$ (orange solid line); the calculations were based on data taken from refs. 10 and 11.

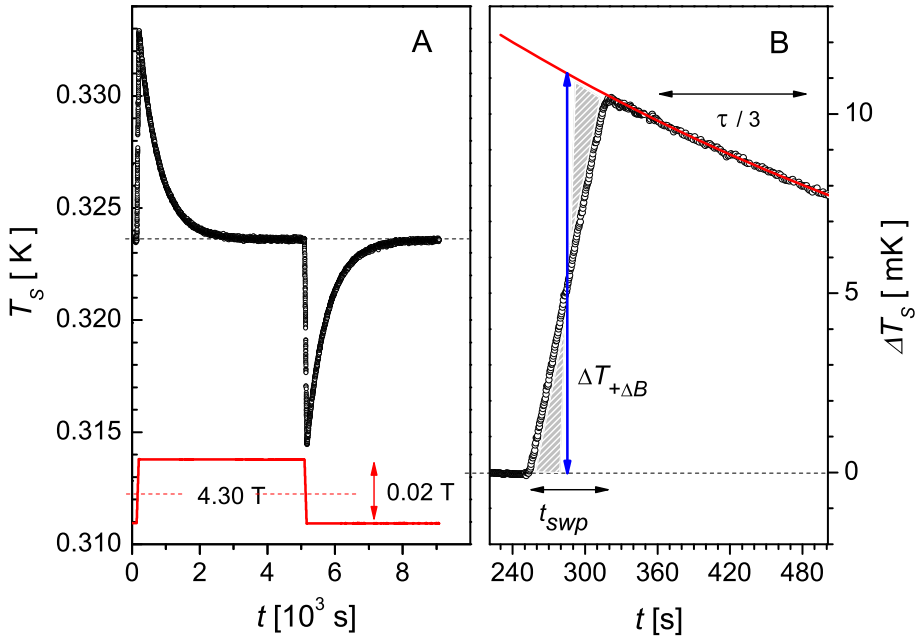

Figure S1

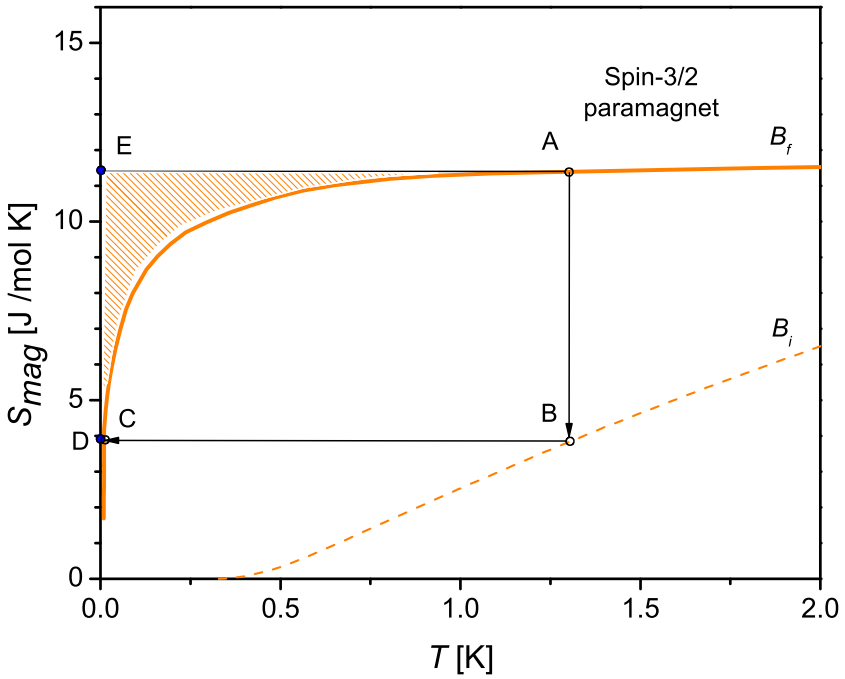

Figure S2